Online Supporting Information

Efficient and Selective CO_2 to CO Electrolysis on Solid Ni-N-C Catalysts at Industrial Current Densities

Tim Möller, [1‡] Wen Ju,[1‡] Alexander Bagger,[2] Xingli Wang,[1] Fang Luo,[1]Trung Ngo Thanh,[1] Ana Sofia Varela,[3] Jan Rossmeisl,[2] and Peter Strasser[1]*

1. The Electrochemical Energy, Catalysis, and Materials Science Laboratory, Department of Chemistry, Chemical Engineering Division, Technical University Berlin, Berlin, Germany
2. Department of Chemistry, University Copenhagen, Universitetsparken 5, 2100 Copenhagen, Denmark
3. Institute of Chemistry, National Autonomous University of Mexico, Mexico City, Mexico

‡Tim Möller and Wen Ju contribute equally

Corresponding author:
Peter Strasser, e-mail: pstrasser@tu-berlin.de;

Experimental sections: Catalysts synthesis and characterization, product analysis

Experimental Section:

Catalysts Synthesis

Preparation of carbon support

Ketjen EC 600JD (AzkoNobel) was stirred in 0.5 M HCl for 24 hours and then rinsed with DI water to reach neutral pH. Afterwards, the dried carbon was refluxed in concentrated nitric acid for 8 hours at 90 °C followed by rinsing with DI water till the pH value turned to 7. After drying at 90 °C in the oven, the carbon will be referred to as carbon support. Before any further utilization in catalyst synthesis, the carbon support was sonicated in 50 mL DI-water till homogenously dispersed.

Synthesis of Fe-N-C

Preparation of the Fe-N-C follows a procedure published in Ref[1]. 3 ml of aniline, 5 g iron chloride ($FeCl_3$) and 5 g ammonium persulfate (APS, $(NH_4)_2S_2O_8$) was added to 0.5 L of 1 M HCl and stirred for one hour. Then, the suspension was stirred for 48 hours along with 0.4 g of dispersed carbon support. Afterwards, the suspension was dried at 95 °C for 24 hours. After drying, the solid mixture was ball-milled in a Zr_2O_3 container with Zr_2O_3 balls (ball diameter 1 cm). Heat treatment (HT) was performed in a furnace with a ramp of 30°C min^{-1} to 900 °C and kept at this temperature for 1 hour within N_2 atmosphere (flow rate: 30 ccm). After cooling down, the material was washed in 2 M sulfate acid (AW) overnight and rinsed to neutral pH by use of vacuum filtration. An HT-AW- HT-AW-HT-procedure was performed to obtain the final Fe-N-C catalyst.

Synthesis of Ni-N-C

The synthesis of Ni-N-C is analogous to the Fe-N-C preparation but $NiCl_2$ is used as metal precursor and one additional AW-HT cycle is performed compared to Fe-N-C.

Note: Distinct from iron, metallic nickel has a special interaction with carbon species. This is why nickel is commonly used as a catalyst for nanotube growth.[2, 3] Taking this into consideration, Ni particles formed during the synthesis are likely to be further covered and encapsulated by the carbon matrix. This results in the formation of acid-unsolvable Ni particles, protected by a carbon layers and strong signals in the XRD from a crystalline phase (Fig. S1). In Figure S2, we measured that the thickness of the dense carbon layer is over 10 nm, denying the corrosion by the acid-

treatments during the synthesis steps, while simultaneously blocking any catalytic reactivity of such particles as well as the XPS detection (on the crystalline).

Synthesis of metal free N-C

The synthesis of the metal free PANI (N-C) starts with an identical route to the Fe-N-C preparation but does not involve any metal precursor. The N-C catalyst is obtained after the first HT and does not involve any AW steps.

Physical and Chemical Characterization

Powder X-ray diffraction (PXRD) patterns were recorded with Bruker D8 Advance instrument with Cu Kα radiation (λ = 1.54056 Å) in the 2θ range of 10-90°. Transmission Electron Microscopy (TEM) was performed using a FEI Tecnai G2 Microscope 20 S-Twin with a LaB6-cathode at 200 kV accelerating voltage (ZELMI Centrum, Technical University of Berlin). The samples were ultrasonicated in ethanol and drop-casted onto Cu-grids. Corresponding analysis was done using software from ImageJ. Specific surface area was obtained from N_2 physisorption measurements conducted on an Autosorb-1 (Quantachome Instruments) using Brunauer-Emmett-Teller (BET) theory and the electrochemical double layer capacitance of the 3 PANI candidates was measured in N_2 saturated neutral potassium hydrogenphosphate solution (0.05 M K_3PO_4 + 0.05 M H_3PO_4, pH = 6.9) at the scan rate 15 mV s^{-1}, 10 mV s^{-1}, 5 mV s^{-1} and 1 mV s^{-1}. CO chemisorption measurements were performed using "Thermo Scientific TPD/R/O 1110". For each measurement, 100–150 mg of the as prepared catalyst was loaded in the sample chamber and the tests were performed in helium atmosphere (He flow: 20 ccm) at −80 °C with six CO pulses. Bulk metal content was measured with Inductively Coupled Plasma Optical Emission Spectrometry (ICP-OES). X-ray photoelectron spectroscopy (XPS) measurements was performed using Thermo Scientific K-Alpha$^+$ X-ray Photoelectron Spectrometer. All samples were analyzed using a microfocused, monochromated Al K α X-ray source (1486.68 eV; 400 μm spot size). The K-Alpha$^+$ charge compensation system was employed during analysis to prevent any localized charge buildup. The N1s spectra was analyzed using the software CasaXPS.

Density Function Theory Calculation

The M-N-C models were created in ASE by a 3 × 5 unit cell of graphene with a functionalized Metal-N_4 site, having the outmost carbon atoms fixed in position and periodic boundaries were applied. Furthermore the Ag(111) structures was made by a 3 x 3 x 3 slab model, with the two lower layers fixed and periodic boundaries. The electronic calculations were carried out with the GPAW software[4] with the projector augmented wave method, spin polarization for the M-NC models and the revised Perdew–Burke–Ernzerhof (RPBE) functional.[5] We applied a 0.18 grid spacing together with a (2 × 2 × 1) and (4 × 4 × 1) k-point sampling for the M-NC and the Ag(111) slab. All the structures were relaxed to a force below 0.1 eV/Å. The free energy diagrams were calculated using the hydrogen electrode[6] and thermodynamic values from reference.[7] The

functional error of the calculated CO_2 RPBE energy was corrected by 0.45 eV together with a -OH water correction of 0.25 eV and a *CO water correction of 0.1 eV.[8]

Electrochemical Characterization with H-Cell

A catalyst ink was produced with 15 mg catalyst, 150 µl isopropanol, 800 µl DI water, and 50 µl 5 wt.% Nafion perfluorinated resin solution (Sigma-Aldrich). After the dosing and mixing, the ink suspension was sonicated using an ultrasonic horn for 8 minutes. 50 µl of ink were deposited onto glassy carbon with 1 cm^2 area resulting in a catalyst loading of 0.75 mg cm^{-2}. The catalyst ink of the reference AgO_x (Sigma-Aldrich, Ref. Nr.:223638) sample was prepared analogously. The prepared electrode was inserted into a CO_2-saturated, 0.1 M $KHCO_3$ solution (Honeywell) in a two compartments, home-made H-cell, divided by an anion exchange membrane (Selemion AMV, AGC Engineering Co., LTD). The electrochemical reduction reaction is controlled using a SP-300 potentiostat (Biologic). 50% of the ohmic drop was automatically corrected and the rest was corrected manually. Before the bulk CO_2 electrolysis, a Linear Sweep Voltammetry step (LSV) was performed at the scan rate 5 mV s^{-1} from -0.1 V vs. RHE towards the desired working potential and then kept the potential constant for 60 minutes.

CO_2 Reduction in Micro Flow Cell

Measurements at high current densities were performed in a commercial Micro Flow Cell (MFC) supplied by ElectroCell. In all Flow-Cell experiments a commercial Ir-MMO plate (ElectroCell) was used as anode. The catalyst-inks were spray-coated on the microporous layer (MPL) of a Freudenberg C2 gas diffusion layer (GDL) on a geometric area of 3 cm^2 to achieve a catalyst loading of 1 mg cm^{-2}. Nafion (Sigma-Aldrich, 5 wt% resin solution) was used as binder and for ionic conductivity of the catalyst-layer. For usual fabrication of the respective inks 6 mg of the AgO_x catalyst, or 15 mg of the M-N-C powders were dispersed with 60 µl Nafion solution in a mixture of Milli-Q water and isopropanol. An aqueous solution of 1 M $KHCO_3$ was used as anolyte and catholyte, which were separated by an anion exchange membrane (Selemion AMV, AGC Engineering Co., LTD.). Both electrolytes were cycled through each respective compartment at 100 mL min^{-1}. The CO_2 feed was supplied at rate of 50 mL min^{-1} to the cathode and was flown from the back of the carbon paper through the catalyst-layer. Measurements were performed

galvanostatically for two hours at each respective current during the catalytic tests, sweeping the current from low to high values.

Products Quantification

The gas (CO_2: 99.999%) was continuously purged into the cell and the exhaust was directly introduced to the Online GC (Shimadzu GC 2014) for H-Cell experiments, whereas the catholyte/gas mixture was returned to the catholyte reservoir first, in the Flow-Cell, from where sampling was performed. Gas products were analyzed at 15 and 60 minutes (H-Cell) or every 30 min (Flow-Cell) of bulk electrolysis by Flame Ionization Detector (FID, for CO, CO_2, CH_4 and C_2H_4) and Thermo Conductivity Detector (TCD, for H_2, O_2 and N_2). After the reaction, the electrolyte was injected in HPLC (Agilent 1200, Detector: RID, for formate) and liquid GC (Shimadzu 2010 plus, Detector: FID, for alcohols) for liquid products quantification. Calculation details are presented in the Supplementary Equations S1-S4.

Equation S1. Production Rate of Gas Products

$$\dot{n} = \frac{\dot{V} * C}{A * V_M}$$

$\dot{n}$: *Generation rate of the product / mol s^{-1} cm^{-2}*

$\dot{V}$: *CO_2 gas flow rate / L s^{-1}*

C: Concentration of the product detected by GC - Volume fraction

A: Geometric area of the electrode / cm^{-2}

V_M: *Molar Volume / 22.4 L mol^{-1}*

Equation S2. Faradaic Efficiency of Gas Products

$$FE = \frac{\dot{n} * z * F}{j_{total}} * 100\%$$

$\dot{n}$: *Generation rate of the product / mol s^{-1} cm^{-2}*

FE: Faradaic Efficiency of the product / %

z: Charge transfer of each product

F: Faradaic Constant / C mol^{-1}

j_{total}: *Total current density during CO_2 bulk electrolysis / A cm^{-2}*

Equation S3. Partial current density

$$j_x = \frac{FE_x * j_{total}}{100}$$

j_x: *Patial current density / mA cm^{-2}*

FE: Faradaic Efficiency of the product / %

j_{total}: *total current density / mA cm^{-2}*

Equation S4. RHE potential

$$E_{RHE} = E_{Ref} + E_{Ag/AgCl} + 0.059 * pH + U * I$$

E_{RHE}: *RHE potential / V*

E_{Ref}: *Applied potential against the reference electrode / V*

$E_{Ag/AgCl}$: *Potential of the reference electrode measured against NHE (0.21 V) / V*

pH: pH-value of the electrolyte

U: Ohmic resistance between working and reference electrode / Ω

I: Total Current of the experiment

Physical and Chemical Characterizations

Table S1. Physical and chemical Characterizations

Sample	a) BET $m^2 g^{-1}$	b) DL-Capa $\mu F\ cm^{-2}$	c) Metal content wt.% (ICP)	d) Metal ratio $\%_{Mole}$ (XPS)	N ratio $\%_{Mole}$	O ratio $\%_{Mole}$	S ratio $\%_{Mole}$	C ratio $\%_{Mole}$	e) CO uptake $mmol\ g^{-1}$
Fe-N-C	634	72.4	1.05	0.82	5.93	3.55	0.53	88.92	60
Ni-N-C	238	22.5	10.2	0.38	3.67	1.91	1.17	92.88	0
N-C	174	25.3	--	--	6.68	3.39	1.03	88.9	0

a) BET: N_2 ad/desorption-based surface area; b) Double layer capacity values, geometric area of each electrode is 1 cm^2 with 0.75 mg cm^{-2} catalyst loading; c) Overall metal content determined from ICP-OES measurement. d) Interfacial atomic ratio quantified with X-ray photoelectron spectra. e) CO uptake at -80°C based on CO chemisorption measurement.

X-Ray Diffraction:

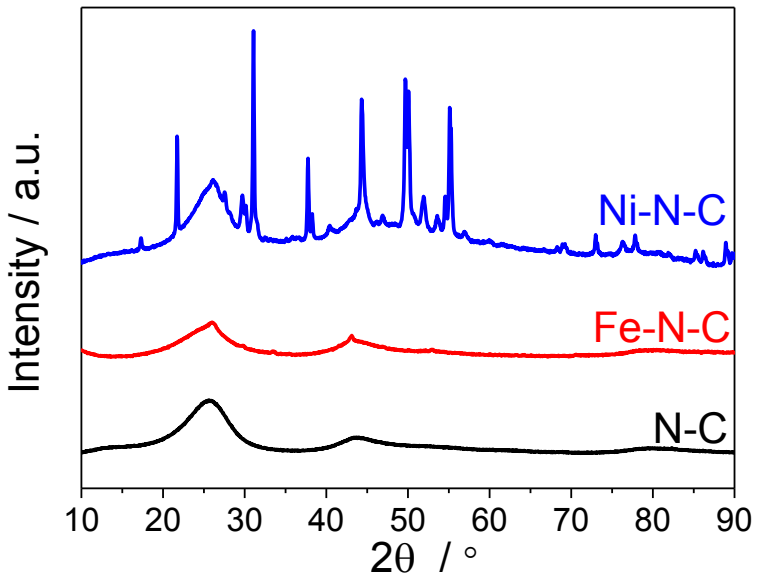

Figure S1. Powder XRD patterns of N-C, Fe-N-C and Ni-N-C catalysts.

TEM image of encapsulated crystalline nanoparticles in Ni-N-C catalyst

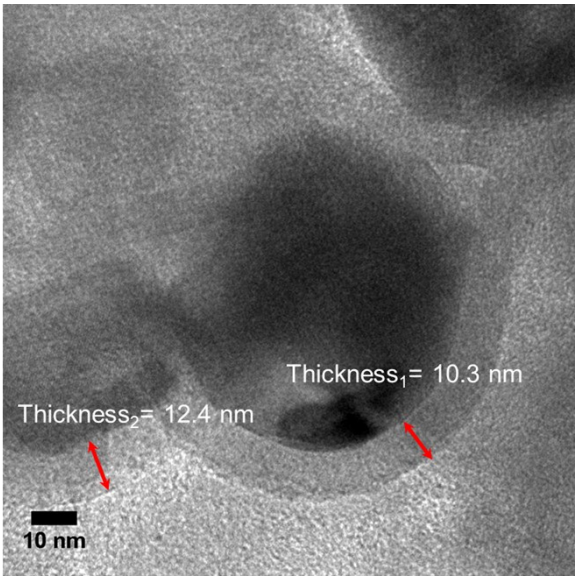

Figure S2. HR-TEM image of carbon-encapsulated crystalline nanoparticles in Ni-N-C catalyst.

BET surface area and Pore size distribution:

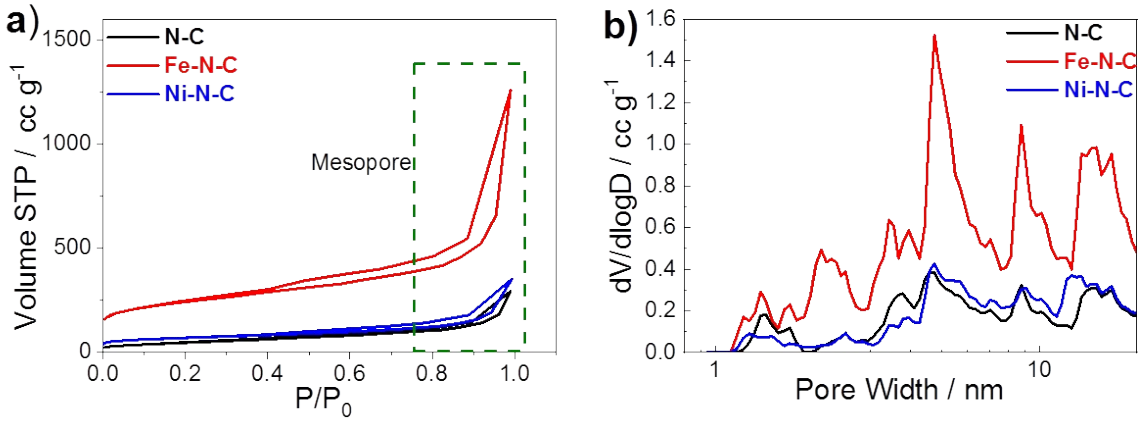

Figure S3. a) N_2 specific ad/desorption isotherm profile; b) pore size distribution of the N-C, Fe-N-C and Ni-N-C catalysts.

Interfacial surface area determination: BETSA vs. ECSA

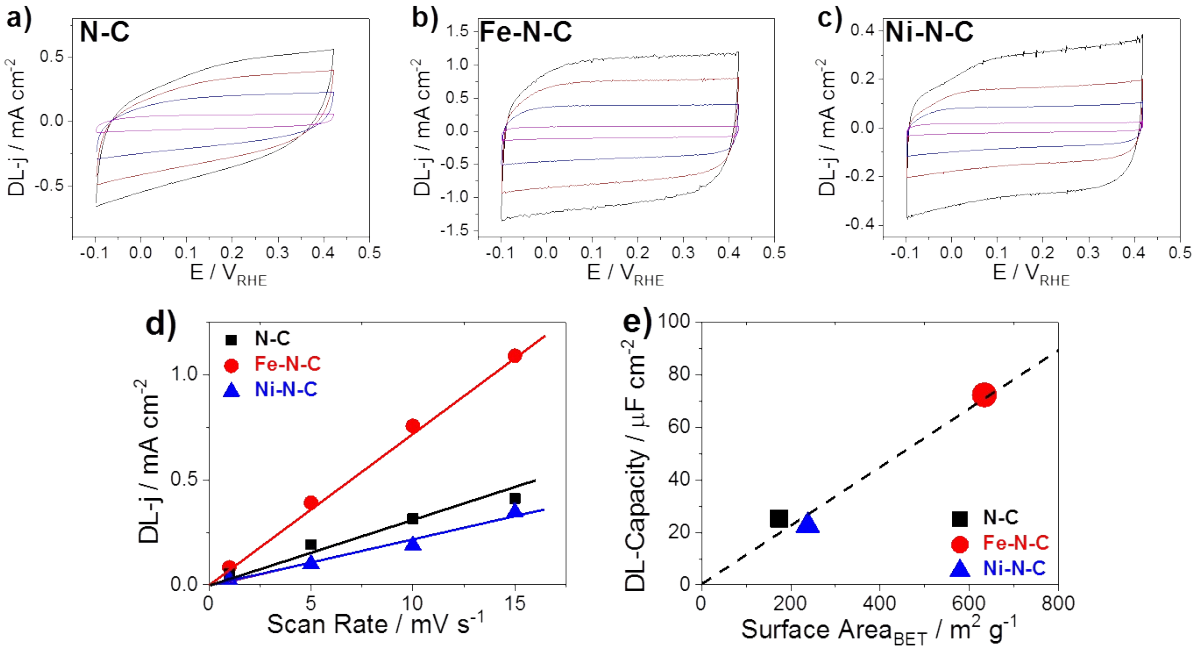

Figure S4. Cyclic voltammetry of a) N-C, b) Fe-N-C and c) Ni-N-C catalysts conducted in N_2-saturated 0.05 M K_2HPO_4 + 0.05 M KH_2PO_4 (pH=6.9) solution at scan rate 15 mV s^{-1}, 10 mV s^{-1}, 5 mV s^{-1}, 1 mV s^{-1} to determine the double layer capacity. Potential was scanned between -0.1 and 0.42 V vs. RHE. d) Double layer current densities (extracted at +0.16 V_{RHE}) on N-C, Fe-N-C and Ni-N-C catalysts at each scan rate. e) Correlation of double layer capacity (ECSA) and the N_2 adsorption derived BET surface area (BETSA). Catalysts loading: 0.75 mg cm^{-2}.

X-ray Photoelectron spectra:

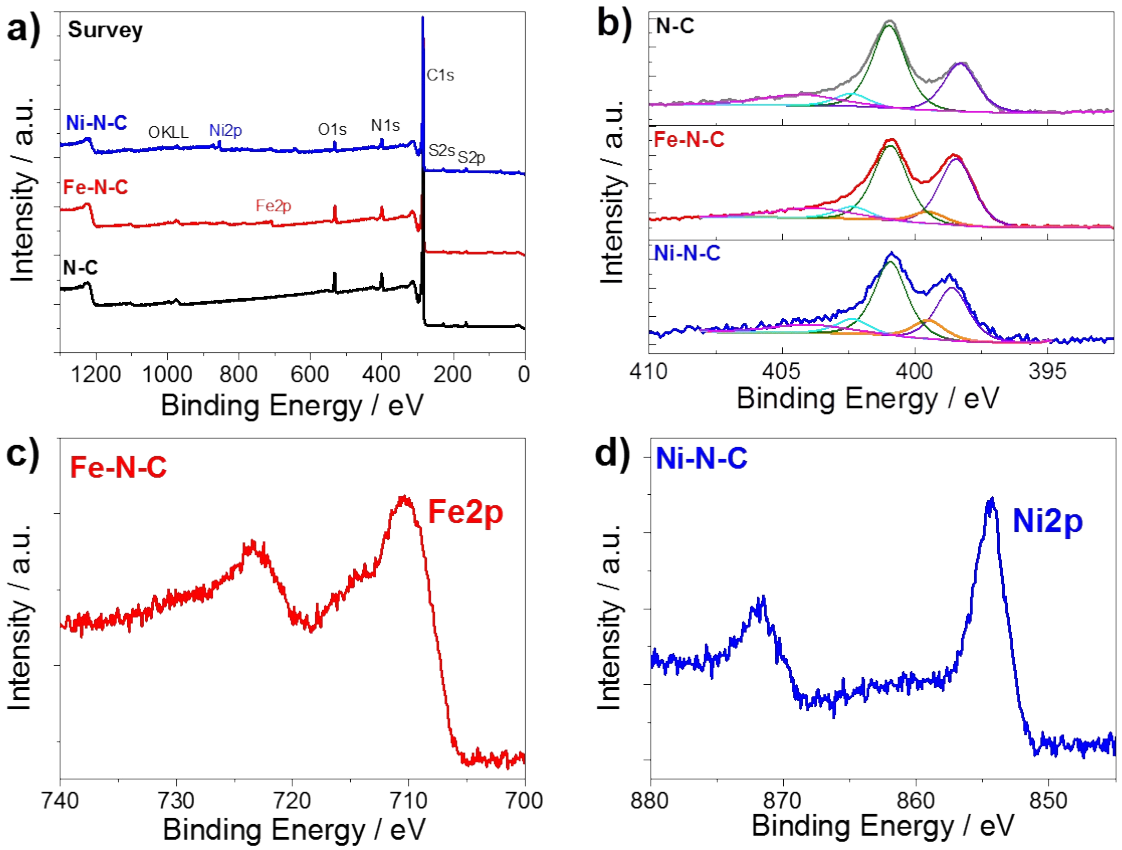

Figure S5. X-ray photoelectron spectra. a) Survey XPS spectra of the PANI derived materials with the main features assigned and high resolution spectra of b) N1s of M-N-C catalysts according to the peak positions: M-N_x moieties (399.7 eV), pyrrolic (401.3 eV), pyridinic (398.6 eV), quaternary (402.5 eV), and graphitic (403.9 eV) according to ref[9-11] c) Fe2p assignment of Fe-N-C and d) Ni2p of Ni-N-C. Please note, XPS data on Fe-N-C and N-C catalysts were already reported in ref[12,13] but measured with other spectrometers.

Electrochemical CO_2RR in H-cell

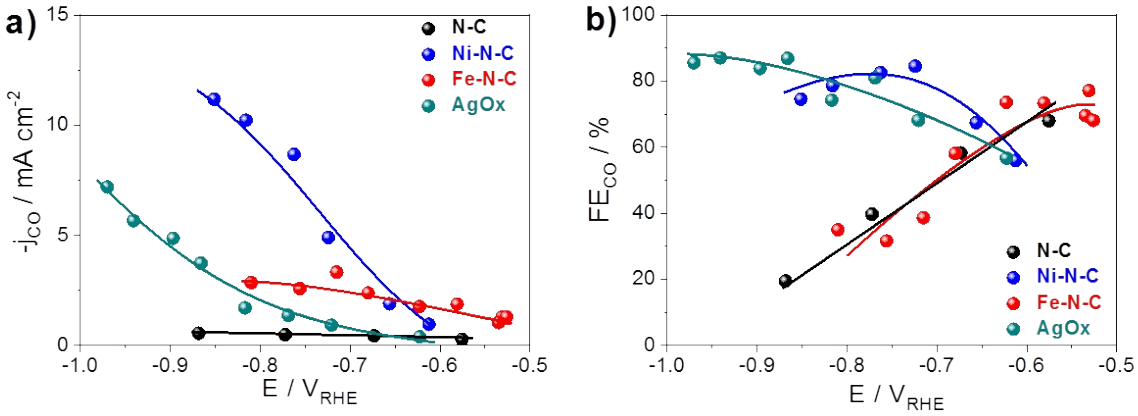

Figure S6. a) Geometric CO production current densities and b) CO faradaic efficiency as a function of applied IR-corrected electrode potential. Lines to guide the eye. Conditions: 60 min at constant electrode potential in CO_2-saturated 0.1 M $KHCO_3$ with 0.75 mg cm^{-2} catalysts loading.

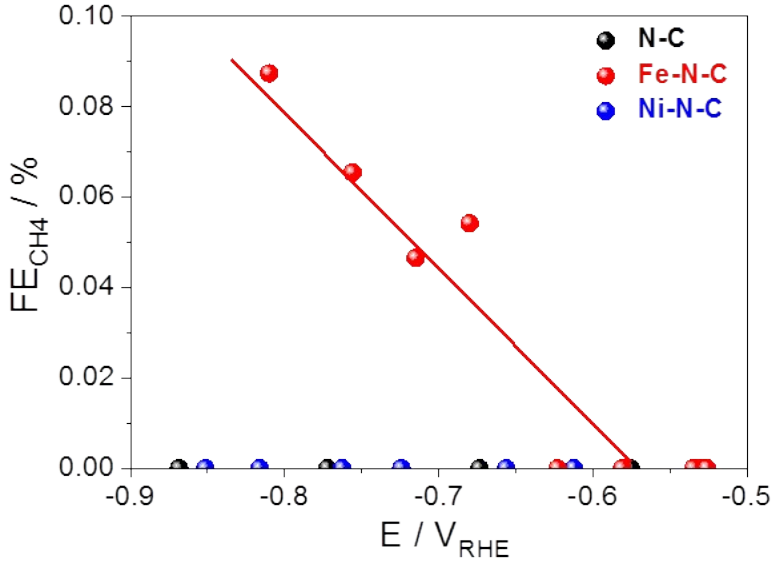

Figure S7. Faradaic efficiency of CH_4 as a function of applied IR-corrected electrode potential. Lines to guide the eye. Conditions: 15 min at constant electrode potential in CO_2-saturated 0.1 M $KHCO_3$ with 0.75 mg cm^{-2} catalysts loading.

DFT calculation of different Ni-Nx-C coordination motifs

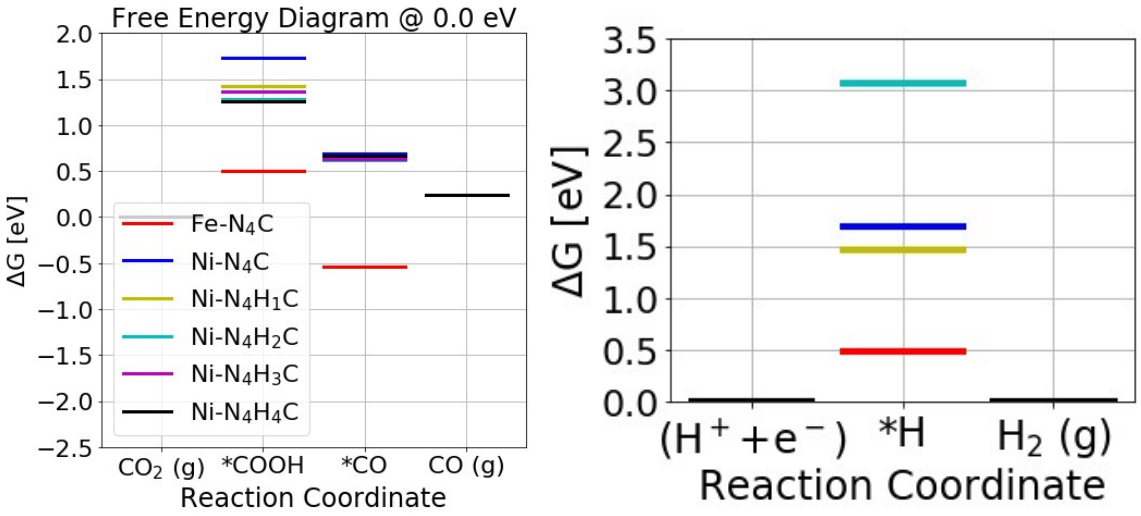

Figure S8. Free energy diagram of CO_2 reduction to CO on the Ni-N-C and Fe-N-C catalysts. Influence of hydrogenating the Ni-N_4-C on the binding strength for the *COOH and *CO intermediate.

Polarization curve and partial CO current in the MFC:

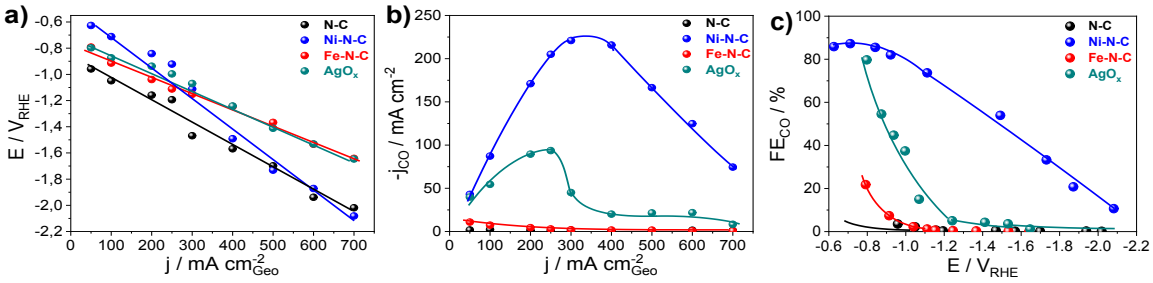

Figure S9. Catalytic testing in flow-cell under current control on N-C (black), Fe-N-C (red), Ni-N-C (blue) and AgO_x (cyan) catalyst. IR-corrected polarization curve (a), partial current for CO formation as a function of current density (b) and CO faradaic efficiency as a function of iR-corrected potential (c). Catalyst loading of 1 mg cm^{-2} on a total GDE active geometric area of 3 cm^2 in CO_2 saturated 1 M $KHCO_3$. Lines to guide the eye.

SEM measurements of the Ni-N-C and AgOx GDE before and after reaction in the MFC:

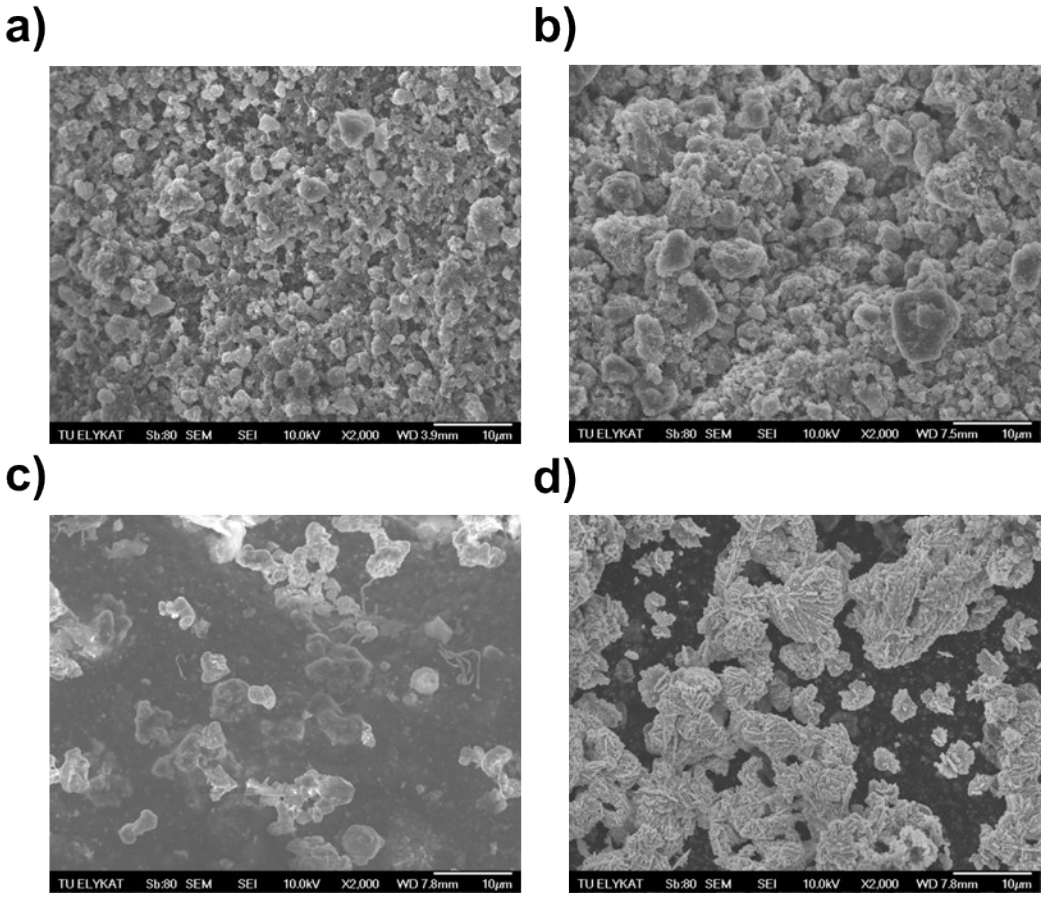

Figure S10. SEM images of the Ni-N-C catalyst before (a) and after (b) electrolysis, as well as the silver catalyst before (c) and after (d) electrolysis. In both cases, testing was performed in the MFC.

Stability test of Electrochemical CO_2RR in the MFC:

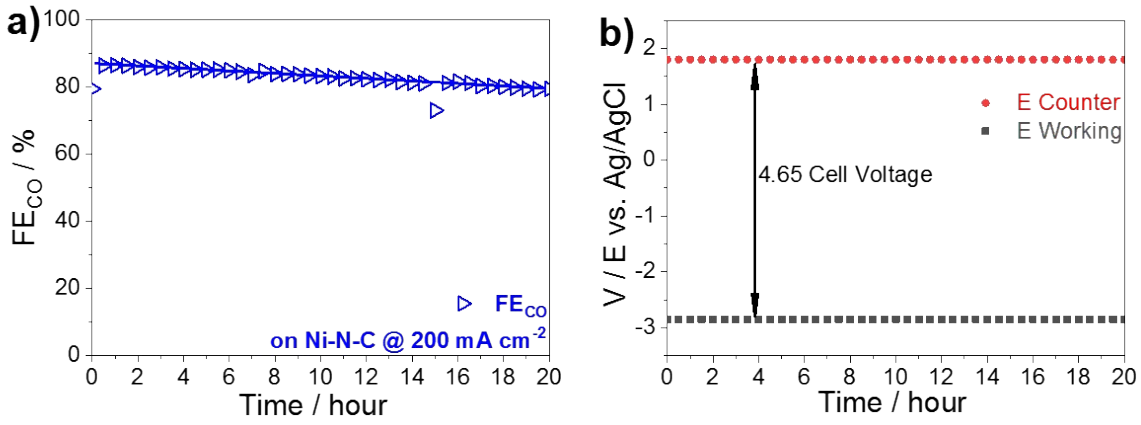

Figure S11. Stability test of Ni-N-C GDL for CO_2RR on in MFC. a) Faradaic efficiency of CO and b) Cell potential (voltage) as a function of stationary electrolysis time. Conditions: 20 hours at constant 200 mA cm^{-2} working current density in CO_2-saturated 1 M $KHCO_3$ with 1 mg cm^{-2} catalysts loading and 3 cm^2 total geometric electrode area. Line to guide the eye.

Table S2: Summary table of the catalytic performance towards CO_2RR referred to Gas Diffusion Electrode.

Catalysts	Electrolyte	Reported condition	Potential (V_{RHE})	Product efficiency	Reference
NOBLE METAL REFERENCE: **Ag**-based GDE Cat. Loading: Not given	1.5M $KHCO_3$/ 0.1 M K_2SO_4	***300 mA cm^{-2} Working current***		FE_{CO}: ~80 % j_{CO}: 240 mA cm^{-2}	[14]Schmid
NOBLE METAL REFERENCE: CD-**Ag**/PTFE Cat. Loading: Not given	1 M $KHCO_3$	***Over 150 mA cm^{-2} Working current***	-1.2	FE_{CO}: 90 %	[15]Sargent
	1 M KOH		-0.8	FE_{CO}: 90 %	
M-N-C Candidates: Ni-GS Cat loading: 0.2 mg cm^{-2}	0.5 M $KHCO_3$	***-0.75 V vs. RHE Working current below 60 mA cm^{-2}***	-0.75	FE_{CO}: 90% j_{Co}: ~54 mA cm^{-2} j: 60 A g^{-1}	[16]Jiang et al.
M-N-C Candidates: Ni-PANI Cat loading: 1 mg cm^{-2}	1 M $KHCO_3$	***50 to 700 mA cm^{-2} Working current***	-0.9	CO: ~85% j_{CO}: > 200 mA cm^{-2} (> 200 A g^{-1})	**This work**

References:

1. N. Leonard, W. Ju, I. Sinev, J. Steinberg, F. Luo, A. S. Varela, B. Roldan Cuenya and P. Strasser, *Chem Sci*, 2018, **9**, 5064-5073.
2. R. Atchudan, J. Joo and A. Pandurangan, *Materials Research Bulletin*, 2013, **48**, 2205-2212.
3. Z. Wang, H. Ogata, S. Morimoto, J. Ortiz-Medina, M. Fujishige, K. Takeuchi, H. Muramatsu, T. Hayashi, M. Terrones, Y. Hashimoto and M. Endo, *Carbon*, 2015, **94**, 479-484.
4. J. Enkovaara, C. Rostgaard, J. J. Mortensen, J. Chen, M. Dułak, L. Ferrighi, J. Gavnholt, C. Glinsvad, V. Haikola, H. A. Hansen, H. H. Kristoffersen, M. Kuisma, A. H. Larsen, L. Lehtovaara, M. Ljungberg, O. Lopez-Acevedo, P. G. Moses, J. Ojanen, T. Olsen, V. Petzold, N. A. Romero, J. Stausholm-Møller, M. Strange, G. A. Tritsaris, M. Vanin, M. Walter, B. Hammer, H. Häkkinen, G. K. H. Madsen, R. M. Nieminen, J. K. Nørskov, M. Puska, T. T. Rantala, J. Schiøtz, K. S. Thygesen and K. W. Jacobsen, *Journal of Physics: Condensed Matter*, 2010, **22**, 253202.
5. B. Hammer, L. B. Hansen and J. K. Nørskov, *Physical Review B*, 1999, **59**, 7413-7421.
6. J. K. Nørskov, J. Rossmeisl, A. Logadottir, L. Lindqvist, J. R. Kitchin, T. Bligaard and H. Jónsson, *The Journal of Physical Chemistry B*, 2004, **108**, 17886-17892.
7. K. Chan, C. Tsai, A. Hansen Heine and K. Nørskov Jens, *ChemCatChem*, 2014, **6**, 1899-1905.
8. A. A. Peterson, F. Abild-Pedersen, F. Studt, J. Rossmeisl and J. K. Norskov, *Energy & Environmental Science*, 2010, **3**, 1311-1315.
9. K. Artyushkova, B. Kiefer, B. Halevi, A. Knop-Gericke, R. Schlogl and P. Atanassov, *Chem Commun*, 2013, **49**, 2539-2541.
10. S. Kabir, K. Artyushkova, B. Kiefer and P. Atanassov, *Physical Chemistry Chemical Physics*, 2015, **17**, 17785-17789.
11. C. Yan, H. Li, Y. Ye, H. Wu, F. Cai, R. Si, J. Xiao, S. Miao, S. Xie, F. Yang, Y. Li, G. Wang and X. Bao, *Energy & Environmental Science*, 2018, **11**, 1204-1210.
12. N. R. Sahraie, U. I. Kramm, J. Steinberg, Y. Zhang, A. Thomas, T. Reier, J.-P. Paraknowitsch and P. Strasser, *Nature Communications*, 2015, **6**, 8618.
13. N. Leonard, W. Ju, I. Sinev, J. Steinberg, F. Luo, A. Varela, B. Roldan and P. Strasser, *Chemical Science*, 2018, DOI: 10.1039/C8SC00491A.
14. T. Haas, R. Krause, R. Weber, M. Demler and G. Schmid, *Nature Catalysis*, 2018, **1**, 32-39.
15. C.-T. Dinh, F. P. García de Arquer, D. Sinton and E. H. Sargent, *ACS Energy Letters*, 2018, **3**, 2835-2840.
16. K. Jiang, S. Siahrostami, A. J. Akey, Y. Li, Z. Lu, J. Lattimer, Y. Hu, C. Stokes, M. Gangishetty, G. Chen, Y. Zhou, W. Hill, W.-B. Cai, D. Bell, K. Chan, J. K. Nørskov, Y. Cui and H. Wang, *Chem*, 2017, **3**, 950-960.